Accepted Manuscript

Catalytic Cyclohexene Oxidation in the Nano Channels of a Copper Silicate Material

Dong Hyeon Lee, Hyun Sung Kim[*]

Department of Chemistry, Pukyong National University, Busan 48513, Korea

*E-mail: kimhs75@pknu.ac.kr

Correspondence should be addressed to
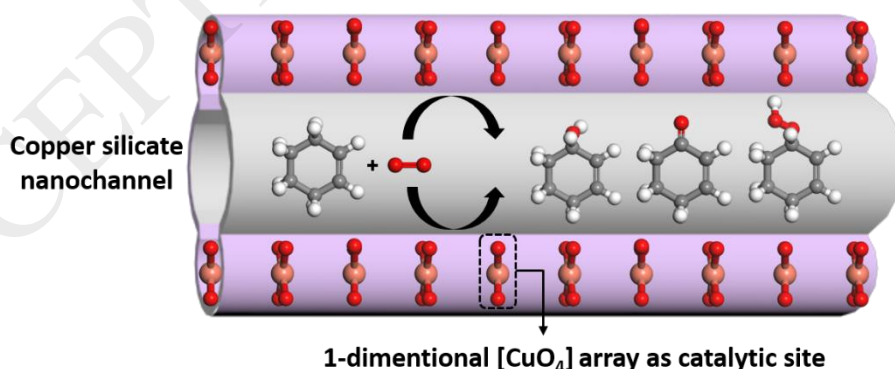
Hyun Sung Kim; kimhs75@pknu.ac.kr

AUTHOR INFORMATION

Corresponding Author

*Hyun Sung Kim. Tel:+82-51-629-5596. Fax:+82-51-629-5583.

 E-mail: kimhs75@pknu.ac.kr

Graphical Abstract

Copper silicate nanochannel

1-dimentional [CuO$_4$] array as catalytic site

Highlights

- Copper silicate, SGU-29 possesses 1-dimensional square planner CuO_4^{2-} unit array in

the framework.

- Square planner CuO_4^{2-} unit works as catalytic active site for aerobic partial oxidation of cycloalkene.

- The molecular sieving effect of SGU-29 for catalytic performance was studied.

- Aerobic partial oxidation of cycloalkene has been investigated to be occurred in nanochannel of SGU-29.

ABSTRACT

Herein we examined the catalytic activity of the copper silicate material SGU-29 for the aerobic partial oxidation of cyclohexene under mild conditions (1 bar of O_2 at 70 °C). In particular, the catalytic properties of the active sites provided by [CuO_4] square planar units in SGU-29 were investigated for cyclohexene oxidation to generate three main oxidation products (i.e., 2-cyclohexene-1-ol, 2-cyclohexene-1-one, and cyclohexene hydroperoxide). Based on the molecular sieving effect of SGU-29, we especially investigated the intrazeolitic reaction, a catalytic cyclohexene oxidation occurring only in nanochannels of SGU-29. A conversion yield of 42.2% was obtained for the aerobic cyclohexene oxidation occurring only in SGU-29 nanochannels under 1 bar of O_2 at 70 °C for 12 h. We demonstrated unequivocally that catalysis occurred only within the inner channels of SGU-29, rather than on its external surface or within the solvent, and we highlighted the special role of [CuO_4] square planar units in catalysis.

Introduction.

In the fine chemical industry, the allylic oxidation of olefins has gained crucial importance in activating raw chemicals to form high value–added intermediates [1-4]. One class of raw materials used in this regard is cyclic olefins such as cyclohexene. Cyclohexene can be oxidized to a variety of oxygen–containing derivatives depending on the type of oxidant used in the reaction. For example, cyclohexene can form epoxy cyclohexane or adipic acid if

hydroperoxide [5,6], NaOCl [7,8], or PhIO [9,10], are used as the oxidant. Additionally, use of the bulky tert–butyl hydroperoxide (TBHP) [11-15] as the oxidant for cyclohexene oxidation gives 2–cyclohexene–1–ol and 2–cyclohexene–1–one, which are important intermediates in the fragrance industry and organic synthesis. However, these aforementioned oxidants are environmentally unfriendly and increase production costs due to their hazardous nature and the need for additional purification steps. In terms of the environment, oxygen is an ideal green oxidizing agent since it is free, forms water as the only by–product, and contains the maximum oxidizing weight percentage [16]. Until now, much progress has been made on the aerobic oxidation of cyclohexene, particularly using noble metal nanoparticles [17,18], carbon nanotubes [19], and mesoporous materials [20,21]. However, for heterogeneous catalytic systems, there are still many aerobic oxygenation reactions for which a general catalyst has yet to be found. Yet as interest in this area increases, the number of studies on these catalysts has grown substantially. One promising class of candidates to function as a heterogeneous catalyst includes microporous materials such as zeolites [22,23] and metal–organic frameworks (MOF) [24-28]. These materials can provide specifically tailored catalytic sites in confined nano–sized spaces, which may not only accelerate chemical reaction rates but also control reactant and product selectivity. In particular, the use of microporous zeotype materials, where a transition metal is substituted into an Al and/or Si atom location in the zeolite framework, has been studied intensively as catalysts. For instance, Potter and co–workers extended the family of transition metal–doped aluminophosphate (AlPO) frameworks [29,30] to obtain isomorphous incorporation of bimetallic active centers that display superior catalytic activity in oxidation reactions

As an important class of zeotypes, the copper silicate material SGU–29 has recently been synthesized and characterized [31,32]. The structure of SGU–29 is noteworthy as it comprises 1–dimensional [CuO_4] square planar units array supported by four surrounding $SiO4$ tetrahedrons, which are arranged almost parallel to each other with distances of 3.629 and 3.732 Å, as shown in Figure 1. The unique structural features of SGU-29 are associated with excellent moisture-independent CO_2 sorption. The vacant space between each [CuO_4] square planar units, which can be termed an intra–crystalline copper(II) center, is able to deliver a specific catalytic function for various chemical reactions. The effective window size of the channel in SGU–29 is 4.5×7.3 Å, which is sufficient for cyclohexene (estimated size: 5.7×3.8 Å, S1(a) in Supplementary Material) to enter as a substrate for subsequent allylic oxidation. Herein, for the first time, we present the catalytic activity of SGU–29 for aerobic

partial oxidation of cyclohexene under mild conditions.

Experimental

Preparation of SGU-29 (Copper silicate). SGU-29 was synthesized according to the previous report as follows [31]. The silicon source solution was prepared by dissolving sodium silicate (40 g, 10.6% Na_2O, and ~26.5% SiO_2, Sigma-Aldrich), NaOH (1.3 g), KCl (12 g) and NaCl (18.5 g), in distilled deionized water (DDW, 60 g). The mixture was continuously stirred at room temperature for 1 h. Separately, for the preparation of the copper source solution, $CuSO_4$ (9.0 g) was completely dissolved in DDW (30 g) containing conc. H_2SO_4 (1.2 g, 95%). The copper source solution was then slowly added dropwise into the silicon source solution while stirring. The mixture was aged with continuous stirring for 15 h at room temperature, and the pH was adjusted to 10.66 by adding aqueous H_2SO_4 solution (10 mM). ETS-10 (100 mg, ~100 nm size) nanopowders were added as seeds and well dispersed by continuous stirring for 20 min. And the prepared gel was placed into Teflon-lined autoclaves (capacity: 25 ml) and kept in a preheated oven at 220 °C for 24 h in a static condition. After hydrothermal reaction, the light purple crystals obtained were collected by centrifugation at 9000 rpm, and washed with copious amounts of water until the pH of the supernatant solution was neutral. The collected SGU-29 powder sample was dried at 80 °C for 6 h in the oven.

Catalytic test for cyclohexene aerobic oxidation.

Cyclohexene oxidation was performed in a magnetically stirred 25-mL Teflon-lined autoclave reactor with integrated K-type thermocouple and pressure gauge (Berghof, model: BR-25). The probe of the thermocouple was submerged in the reactant liquid to measure the real reaction temperature. Typically, 4.0 g of cyclohexene, 4.8 g of acetonitrile, and 1.0 g of toluene as an internal standard and 0.01 g of untreated SGU-29 powder as the catalyst were placed in the Teflon reaction vessel and tightly sealed in the autoclave reactor. Before reaching the desired reaction temperature, the reactor was flushed several times with high-purity (99.999%) N2. Then, the reactor was heated and stabilized at the desired temperature; subsequently, high-purity (99.999%) O_2 was fed into the reactor to maintain the desired pressure. After oxidation was terminated, the reactor was quickly cooled in water, and the oxygen was released until ambient pressure was reached.

The catalyst was removed from the reaction mixture by centrifugation and the products in the supernatant solution were analyzed by gas chromatography (model: Agilent 5890 series II)

equipped with a flame ion detector (FID). In detail, a quantitative determination of the reactant consumed (i.e., cyclohexene) and the oxidation products (i.e., cyclohexene oxide, 2-cyclohexene-1-ol, 2-cyclohexene-1-one, and cyclohexenyl hydroperoxide) was achieved using standard calibration curves. (S2 in Supplementary Material) For examples, the calibration curves for cyclohexene was realized by adding variable concentrations of the corresponding cyclohexene to diethyl ether (0.1mL, 0.45, 0.90, 1.35, 1.80, and 2.70 mM, respectively). The mixture was added with the internal standard (toluene, 0.1 mL from a 0.6 mM stock solution) and analyzed by GC.

To determine the content of cyclohexenyl hydroperoxide, the samples were analyzed twice, before and after reducing cyclohexenyl hydroperoxide to 2-cyclohexene-1-ol with triphenyl phosphine (Acros, 99%) according to previous reports. [33]

Instrumental Analysis. Scanning electron microscopy (SEM) images of pristine SGU-29 and catalytic reacted microcrystal were obtained with FE-SEM (MIRA 3 LMH In-Beam Detector, TESCAN) at an acceleration voltage of 40 kV. X-ray diffraction (XRD) patterns for the identification of the SGU-29 were obtained with X-Ray Diffractometer (PHILIPS/X'Pert-MPD System) using Ni-filtered monochromatic Cu Kα radiation. N_2 adsorption-desorption isotherms were measured in a BELsorp-Max (BEL, JAPAN) at 77 K. The surface areas and pore sizes of the samples were calculated using the Brunauer–Emmett–Teller (BET) and nonlocal density functional theory (NL-DFT) model with the slit pore geometry method, respectively. X-ray photoelectron spectroscopy (XPS) studies were carried out using a VG Multilab 2000 spectrometer (Thermo VG Scientific, UK) using an Al Kα excitation source with a photon energy of 1487 eV. The data was acquired in the hybrid mode.

Electron paramagnetic resonance (EPR) spectra were collected with a Bruker (EMXplus-9.5/2.7) electron spin resonance spectrometer at room temperature, with a frequency of 9.41 GHz and microwave power of 2.00 mW. The center field value was 3348.760 G and sweep width was 400.000 G.

Results and Discussion

Using the procedure described in the Experimental section, we synthesized microporous SGU–29 with a square bipyramidal crystal morphology, as shown by the scanning electron microscopy (SEM) images in Figure 2a. The crystallinity and purity of SGU–29 were confirmed by XRD analysis (Figure 2b.); the patterns obtained matched well with those reported previously [31]. On the basis of Brunauer–Emmett–Teller (BET) analysis of the N2

adsorption isotherm at 77 K, the surface area of SGU–29 was calculated to be 411m^2/g (Figure 2c.), which is consistent with previous observations [31].

We investigated whether the [CuO$_4$] square planar units in the confined channels of SGU-29 were capable of oxidizing cyclohexene to 2-cyclohexene-1-ol, 2-cyclohexene-1-one, and/or cyclohexene-1-peroxide using oxygen as the oxidant. As a test for catalytic activity, the catalytic performance of SGU-29 for oxidation of cyclohexene under mild reaction conditions (i.e., 1 bar of O$_2$ at 70 °C for 12 h) was evaluated. The cyclohexene conversion yield was 47.8%, and the major product selectivities of 2-cyclohexene-1-ol (1), 2-cyclohexene-1-one (2), and cyclohexene hydroperoxide (3) were found to be 20.1, 46.4, and 27.5%, respectively, as shown in Table 1.

Cyclohexene oxide, which is a well–known oxidative product, formed in such a minute quantity that it could be safely ignored, especially since it formed via a different mechanism from that of 1, 2, and 3.

The oxidation yield includes products from reactions occurring within the channels (denoted as inner zeolitic conversion), on the external surface (denoted as external zeolitic conversion), and in the surrounding solvent (denoted as conversion in solvent), which occurs via an auto-oxidation process as shown Figure 3a. In this way, the obtained conversion yield of 47.8% for 12 h is the sum of the conversion yields of cyclohexene oxidation from these three distinct regions.

In order to distinguish the catalytic effect of the [CuO$_4$] square planar units in the SGU–29 nanochannels, we need to consider only inner zeolitic conversion. To examine this type of conversion, we first hypothesized that each conversion yield of aerobic cyclohexene oxidation corresponded to a specific reaction site, which we investigated by employing control experiments using differently sized radical scavengers. First, the radical nature of the catalytic oxidation of cyclohexene by SGU–29 was verified by testing the effect of the radical scavenger. Specifically, addition of the well–known radical scavenger hydroquinone, whose size (estimated diameter: ~5.3 Å, S1(a) in Supplementary Material) is amenable for entry into the channels of SGU–29, completely suppressed the oxidative conversion of cyclohexene in all three potential catalytic regions, and no oxidation of cyclohexene was apparent. This result clearly indicates that aerobic oxidation proceeds via a radical mechanism.

By comparison, addition of the bulky radical scavenger octadecyl–3–(3,5–di–tertbutyl–4–hydroxyphenyl)–propionate (OBHP, estimated diameter: ~9.5 Å S1(b) in Supplementary Material), whose large size precludes entry into the SGU–29 window channel (4.5 × 7.3 Å),

quenched only the radicals in solution. Therefore, OBHP inhibited conversion of cyclohexene on the external surface of SGU–29 and in the solvent. OBHP could not participate in inhibiting the inner zeolitic conversion of cyclohexene, as its bulky nature precluded its full entry into the channels of SGU–29. With OBHP as the radical scavenger under reaction conditions of 1 bar of O2 at 70°C for 12 h, the obtained conversion yield of cyclohexene was found to be 42.2%, with 23.3, 47.7, and 29.0% product selectivities for 1, 2, and 3, respectively. These values were estimated from pure inner zeolitic conversion for cyclohexene oxidation.

To determine the extent of cyclohexene conversion in the solvent, a control experiment under identical conditions (i.e., 1 bar of O_2 at 70 °C for 12 h) in the absence of SGU-29 was performed. The obtained yield was 4.9%.

In this way, the conversion yield of cyclohexene on the SGU–29 external surface was determined arithmetically as 0.7% ($\approx$ 0%) by subtracting the yields from inner zeolitic conversion and conversion in solvent from the total conversion yield. This indicates that the oxidative conversion of cyclohexene catalyzed by the SGU–29 surface contributes very little to the overall conversion yield. When OBHP was employed in the catalytic reactions, all the results for SGU–29 clearly indicated that a heterogeneous catalytic reaction occurred inside the channel of the SGU–29 frameworks. Figure 3b displays the conversion yield for the three reaction regions.

Consequently, we could determine the catalytic performance of purely inner zeolitic conversion. Table 1 lists the conversion yield and selectivity of main products of aerobic cyclohexne oxidation occurred in nanochannel of SGU-29. Figure 4a. and Table 1. show the inner zeolitic catalytic effect of the reaction time on cyclohexene oxidation with OBHP at 1 bar of O_2 and 70°C. As seen, the conversion yield gradually increased with reaction time as selectivity of the three products changed. The maximum cyclohexene conversion yield was ~52.2% after 24 h. Notably, formation of other by-products such as cyclohexene oxide, adipic acid, and succinate acid from over-oxidation during the reaction was observed to have a low selectivity. Up to 12 h, it was lower than 5%, and as the reaction time increased after 24h, the portion of by-products increased up to 26%. This indicated that over-oxidation of the product occurred, leading to the formation of by–products.

The influence of O_2 pressure on the catalytic performance of SGU–29 in the aerobic oxidation of cyclohexene was also investigated, using various O_2 pressures (from 1 to 4 bar) at 70°C (Figure 4b and Table 1). The conversion yield and sum of the three major products

remained constant above 2 bar of O_2 pressure. Remarkably, in terms of product selectivity, the percentage of the peroxide (3) and by-products in the oxidation product mixture increased with O_2 pressure, and cyclohexene oxide was not detected at high oxygen pressures. Moreover, the ratio of by-products increased. The maximum cyclohexene conversion yield was 46.6% at an O_2 pressure of 4 bar, with the main reaction products being 2–cyclohexene peroxide, followed by cyclohexene–1–one and 2–cyclohexene–1–ol.

The temperature-dependent conversion yields with the three major product selectivities in the SGU-29 channels are shown in Figure 4c and Table 1 under the indicated conditions. The conversion yield increased with temperature, and at 70°, SGU–29 displays an outstanding conversion yield for products 1, 2, and 3; however, the conversion yield does not increase above 80°C, and preformation of byproducts is increased. Interestingly, the number of moles of cyclohexene consumed and the number of moles of the three products does not differ at temperatures of <80 °C, indicating that over-oxidation does not occur.

Ensuring the stability of a catalyst is a crucial consideration for its practical application. To evaluate the stability of SGU–29 for cyclohexene oxidation, recycling tests were performed five consecutive times under identical conditions using molecular oxygen as the oxidant. After each reaction, the catalyst was repeatedly washed with fresh acetonitrile and centrifuged until no reactant and product from the supernatant solution were detected via gas chromatography. The results of these recycling tests are shown in Figure 4d. Clearly, the SGU–29 catalyst exhibits consistent performance, with no appreciable difference in its conversion yield and product selectivity after five consecutive cycles. Further, the structural stability of SGU–29 following consecutive reactions was established by XRD, SEM, and BET analyses, which indicated no significant difference between pristine SGU–29 and that used five times as indicated in Figure 2. This demonstrated that the structural integrity of SGU–29 was well retained, thereby contributing to its excellent continuous catalytic performance.

The reaction rate constants for cyclohexene oxidation over inner SGU–29 conversion and auto–oxidation in acetonitrile were obtained in accordance with the indicated reaction temperatures, which ranged from 40 to 70°C as shown S3(a) in supplementary material. S3(b) displays the corresponding Arrhenius plots for cyclohexene oxidation of the pseudo–first order plot kinetics. The activation energy of inner SGU–29 conversions for cyclohexene oxidation (45.9 kJ mol−1) was much less than that associated with solvo–oxidation (58.5 kJ

mol−1). This indicates that the [CuO$_4$] square planar units in the channels of SGU−29 function as the catalytic active sites for cyclohexene oxidation.

Turnover number (TON), which is defined as the molar ratio of converted substrate to catalyst, is an important parameter to evaluate the catalytic performance of a catalyst. We determined the TON of a [CuO$_4$] square planar units in the SGU−29 channels for oxidation under mild reaction conditions (i.e., 1 bar of O$_2$ at 70°C for 12 h) to be 986 by calculating the molar ratio of the product yield from inner zeolitic conversion to that from the [CuO$_4$] square planar units in the SGU−29 channels. Reported conversation yields and TON values for cyclohexene aerobic oxidation using various types of porous catalysts are listed in Table S1. Notably, the obtained TON value (986) from SGU-29 is higher than those from various embedded transition metal elements in other porous catalysts such as MOF. This demonstrates that SGU-29 with the unique structure of arrays of [CuO$_4$] square planar units possesses superior catalytic performance.

The turnover frequency (TOF) was also calculated to reveal the intrinsic activity of the catalytic site. The TOF of the [CuO$_4$] square planar units in the SGU−29 frameworks were found to be 82.1 h^{-1}. Thus, we were able to obtain the conversion yield, TON, and TOF for the inner zeolitic conversion of cyclohexene using the SGU−29 catalysts under various reaction conditions, as summarized in the procedure for obtaining TON and TOF in S4-Supplementary material.

To clarify the roles of the [CuO$_4$] square planar units as the catalytic sites and the enhancement of the reaction as a result of the confined nanospaces within the SGU−29 framework, we ran control experiments using isostructural zeotypes of SGU−29 such as ETS−10 and AM−6. ETS−10 and AM−6 are a unique class of microporous transition metal oxide silicates that possess a 1−dimensional (1D) quantum wire of MO$_6$ (M = Ti and V) octahedra within their framework (as shown in Figure 1). Structurally, SGU−29 differs from ETS−10 and AM−6 only by having 1D arrays of [CuO$_4$] square planar units instead of 1D quantum wires. As mentioned above, the axial positions of [CuO$_4$] square planar units, which are present in the confined spaces between two [CuO$_4$] square planar units in SGU−29, provide distinct active sites for the SGU−29 catalysts, which are not present in ETS−10 and AM−6. In order to verify the role played by the axial positions of [CuO$_4$] square planar units, we evaluated the catalytic performance of ETS−10 and AM−6 under identical mild reaction conditions (i.e., 1 bar of O$_2$ at 70°C for 12 h). The conversion yields of ETS−10 and AM−6 revealed that they demonstrate minute catalytic activities of 4.5 and 5.0%, respectively

(Figure 5a and entry 14-16 of Table 1). These values are comparable to the extent of conversion via solvo–oxidation (4.9%) in the absence of the catalyst. The negligible catalytic activity arises from the absence of axial active sites around the MO_6 (M= Ti and V) octahedra in ETS–10 and AM–6. Additionally, cyclohexene oxidation did not occur with ETS–10 and AM–6 in the presence of OBHP. These control experiments indicate that the $[CuO_4]$ square planar units in the SGU–29 frameworks are likely to be the active sites for cyclohexene oxidation.

Besides cyclohexene, we tested using other cycloalkene series such as cyclopentene, cycloheptene, and cis-cyclooctene under 1 bar of O_2 at 70 °C for 12 h in the presence of OBHP, as shown in Figure 5a. As seen, cyclopentene and cycloheptene were oxidized within the nanochannel of SGU-29 with conversion yields of 28.5% and 24.0%, respectively as shown in Figure 5b. Because the estimated size of cis-cyclooctene (6.2 × 4.5 Å, as seen S5 in Supplementary material) is almost identical to the window size of SGU-29 (7.3 × 4.5 Å), it is difficult for the cis-cyclooctene molecule to enter the channels of SGU-29. Furthermore, the reactant selectivity of SGU-29 could be confirmed by observing only cyclohexene oxidation during the control experiment conducted by employing the reactant mixture of 1:1 cyclohexene and cis-cyclooctene. As expected, only cyclohexene was oxidized, as shown in Figure 5c.

On the basis of previous literature [34], it appears that the aerobic oxidation of cyclohexene in the presence of SGU–29 proceeds via a classic Haber–Weiss radical–chain sequence mechanism. In terms of the Haber–Weiss oxidation mechanism during the initiation period, an increase in ROOH can also be observed in the SGU–29 catalytic systems. This is then followed by either homolytic or heterolytic cleavage of the O–O bond in ROOH, depending on the oxidation state of $[CuO_4]$ square planar units in the SGU–29 frameworks, as illustrated by the proposed mechanism in Scheme 1.

To determine the change in the chemical oxidation state of Cu as a catalytic center in SGU–29, XPS spectra were recorded for the Cu $2p_{3/2}$ core levels of a pristine SGU–29 sample and for a sample used for five cycles. For Cu $2p_{3/2}$ in the case of pristine SGU–29, the oxidation state of Cu could be defined as +2 from the peak at 933.7 eV, with strong two satellite peaks corresponding to Cu^{2+}, as shown in Figure 6a. On the other hand, in the Cu $2p_{3/2}$ core level spectra of the SGU–29 sample that was used for five cycles, the peak at 932.3 eV corresponding to Cu^+ was observed [35]. We noted that the ratio of Cu^{2+} to Cu^+ increased with the number of consecutive catalytic reactions and remained constant above five cycles

(Figure 6b), which was attributed to the role of the Cu as catalytic sites for peroxide cleavage, as described in Scheme 1. To explore this possibility further, electron spin resonance (ESR) analysis using the radical trap reagent, phenyl–N–t–butylnitrone (PBN), which was used as a free radical spin trapping agent that is capable of forming stable radical adducts, was used to identify the radical intermediates after homolytic/heterolytic cleavage of the ROOH (R=cyclohexenyl) species generated during oxidation.

From Scheme 1, we expect four types of radical adducts to be generated during oxidation. As predicted, the deconvolution of the ESR spectra obtained during oxidation in the presence of SGU–29 revealed four types of spin adducts, corresponding to mixtures of ROO•/PBN, RO•/PBN, R•/PBN (R=cyclohexenyl) which formed as shown in Figure 6a, and O•/PBN from PBN itself oxidation [36]. The ESR spectra of four spin adducts observed were clearly distinguished owing to sufficiently different hyperfine splitting constants, as tabulated in Table S2[37,38].

In contrast, without SGU–29, only two ESR signals corresponding to RO•/PBN and ROO•/PBN from the auto–oxidation products of the ROOH in solution were observed, as shown in Figure 6b. The ESR study indicated that [CuO$_4$] in the SGU–29 initiated the generation of homolytic/heterolytic cleavage of ROOH species to form RO• and ROO• radicals, and accelerated the oxidation of cyclohexene. The mechanistic insight suggested in Scheme 1 is consistent with the above results, which were ascertained through XPS and ESR analyses.

Conclusion

In summary, during our investigation of the catalytic properties of the [CuO$_4$] square planar units in SGU–29 for cyclohexene oxidation, we discovered that cyclohexene is oxidized to 2–cyclohexene–1–ol (1), 2–cyclohexene–1–one (2), and cyclohexene hydroperoxide (3) only within the inner channels of SGU–29, in yields reaching 40% and with TON and TOF of 986 and 82.1 h–1, respectively. Notably, there was no physical or chemical destruction of SGU–29. This is the first effort that examines the catalytic properties of SGU–29 and establishes the [CuO$_4$] square planar units as the active oxidation sites. Overall, we believe that these findings will be of great benefit in utilizing the novel catalytic properties of the [CuO$_4$] units in SGU–29 for application to various organic reactions.

Reference

[1] A. Corma, H. García, Chem. Rev. 102 (2002) 3837–3892.

[2] L. Bayeh, P. Q. Le, U. K. Tambar, Nature 547 (2017) 196–200.

[3] E. J. Horn, B. R. Rosen, Y. Chen, J. Tang, K. Chen, M. D. Eastgate, P. S. Baran, Nature 533 (2016) 77-81.

[4] T. Chantarojsiri, J. W. Ziller, J. Y. Yang, Chem. Sci. 9 (2018) 2567–2574.

[5] K. Li, J. Wang, Y. Zou, X. Song, H. Gao, W. Zhu, W. Zhang, J. Yu, M. Jia, Appl. Catal. A: Gen. 482 (2014) 84-91.

[6] R. D. Oldroyd, J. M. Thomas, T. Maschmeyer, P. A. MacFaul, D. W. Snelgrove, K. U. Ingold, D. D. M. Wayner, Angew. Chem., Int. Ed. Engl. 35 (1996) 2787–2790.

[7] H. Yoon, T. R. Wagler, K. J. O'connor, C. J. Burrows, J. Am. Chem. Soc. 112 (1990) 4568–4570.

[8] D. Chatterjee, A. Mitra, J. Mol. Catal. A: Chem. 144 (1999) 363–367.

[9] A. Stassinopoulos, J. P. Caradonna, J. Am. Chem. Soc. 112 (1990) 7071–7073.

[10] J. C. Medina, N. Gabriunas, E. Páez-Mozo, J. Mol. Catal. A: chem. 115 (1997) 233–239.

[11] M. Tonigold, Y. Lu, B. Bredenkötter, B. Rieger, S. Bahnmüller, J. Hitzbleck, G. Langstein, D. Volkmer, Angew. Chem., Int. Ed. 48 (2009) 7546–7550.

[12] H. Noh, Y. Cui, A. W. Peters, D. R. Pahls, M. A. Ortuño, N. A. Vermeulen, C. J. Cramer, L. Gagliardi, J. T. Hupp, O. K. Farha, J. Am. Chem. Soc. 138 (2016) 14720–14726.

[13] T. Zhang, Y.-Q. Hu, T. Han, Y.-Q. Zhai, Y.-Z. Zheng, ACS Appl. Mater. Interfaces 10 (2018) 15786–15792.

[14] D. Ruano, M. Díaz-García, A. Alfayate, M. Sánchez-Sánchez, ChemCatChem 7 (2015) 674–681.

[15] P. Cancino, V. Paredes-García, P. Aguirre, E. Spodine, Catal. Sci. Technol. 4 (2014) 2599–2607.

[16] F. Nezampour, M. Ghiaci, H. Farrokhpour, Appl. Catal. A: Gen. 543 (2017) 104-114.

[17] J. Dou, F. Tao, Appl. Catal. A: Gen. 529 (2017) 134-142.

[18] Z.-Y. Cai, M.-Q. Zhu, J. Chen, Y.-Y. Shen, J. Zhao, Y. Tang, X.-Z. Chen, Catal. Commun. 12 (2010) 197–201.

[19] Y. Cao, H. Yu, F. Peng, H. Wang, ACS Catal. 4 (2014) 1617–1625.

[20] X. Sang, J. Zhang, T. Wu, B. Zhang, X. Ma, L. Peng, B. Han, X. Kang, C. Liu, G. Yang, RSC Adv. 5 (2015) 67168–67174.

[21] M. B. Ansari, B.-H. Min, Y.-H. Mo, S.-E. Park, Green Chem. 13 (2011) 1416-1421.

[22] R. Raja, G. Sankar, J. M. Thomas, Chem. Commun. (1999) 829–830.

[23] S. Yamaguchi, T. Fukura, K. Takiguchi, C. Fujita, M. Nishibori, Y. Teraoka, H. Yahiro, Catal. Today 242 (2015) 261–267.

[24] G. Tuci, G. Giambastiani, S. Kwon, P. C. Stair, R. Q. Snurr, A. Rossin, ACS Catal. 4 (2014) 1032–1039.

[25] D. Sun, F. Sun, X. Deng, Z. Li, Inorg. Chem. 54 (2015) 8639–8643.

[26] P. Cancino, A. Vega, A. Santiago-Portillo, S. Navalon, M. Alvaro, P. Aguirre, E. Spodine, H. García, Catal. Sci. Technol. 6 (2016) 3727–3736.

[27] Y. Qi, Y. Luan, J. Yu, X. Peng, G. Wang, Chem. – Eur. J. 21 (2015) 1589–1597.

[28] Y. Fu, D. Sun, M. Qin, R. Huang, Z. Li, RSC Adv. 2 (2012) 3309-3314.

[29] M. E. Potter, A. J. Paterson, R. Raja, ACS Catal. 2 (2012) 2446–2451.

[30] J. Paterson, M. Potter, E. Gianotti, R. Raja, Chem. Commun. 47 (2011) 517–519.

[31] S. J. Datta, C. Khumnoon, Z. H. Lee, W. K. Moon, S. Docao, T. H. Nguyen, I. C. Hwang, D. Moon, P. Oleynikov, O. Terasaki, K. B. Yoon, Science 350 (2015) 302–306.

[32] M. K. Song, S. J. Datta, K. B. Yoon, J. Phys. Chem. C 120 (2016) 20206–20215.

[33] G. B. Shul'Pin, J. Mol. Catal. A: Chem. 189 (2002) 39–66

[34] I. M. Denekamp, M. Antens, T. K. Slot, G. Rothenberg, ChemCatChem 10 (2018) 1035–1041.

[35] N. Benito, M. Flores, J. Phys. Chem. C 121 (2017) 18771–18778.

[36] M. Erben, D. Veselý, J. Vinklárek, J. Honzíček, J. Mol. Catal. A: Chem. 353-354 (2012) 13–21.

[37] E. Niki, S. Yokoi, J. Tsuchiya, Y. Kamiya, J. Am. Chem. Soc. 105 (1983) 1498-1503.

[38] D. L. Haire, U. M. Oehler, P. H. Krygsman, E. G. Janzen, J. Org. Chem. 53 (1988) 4535–4542.

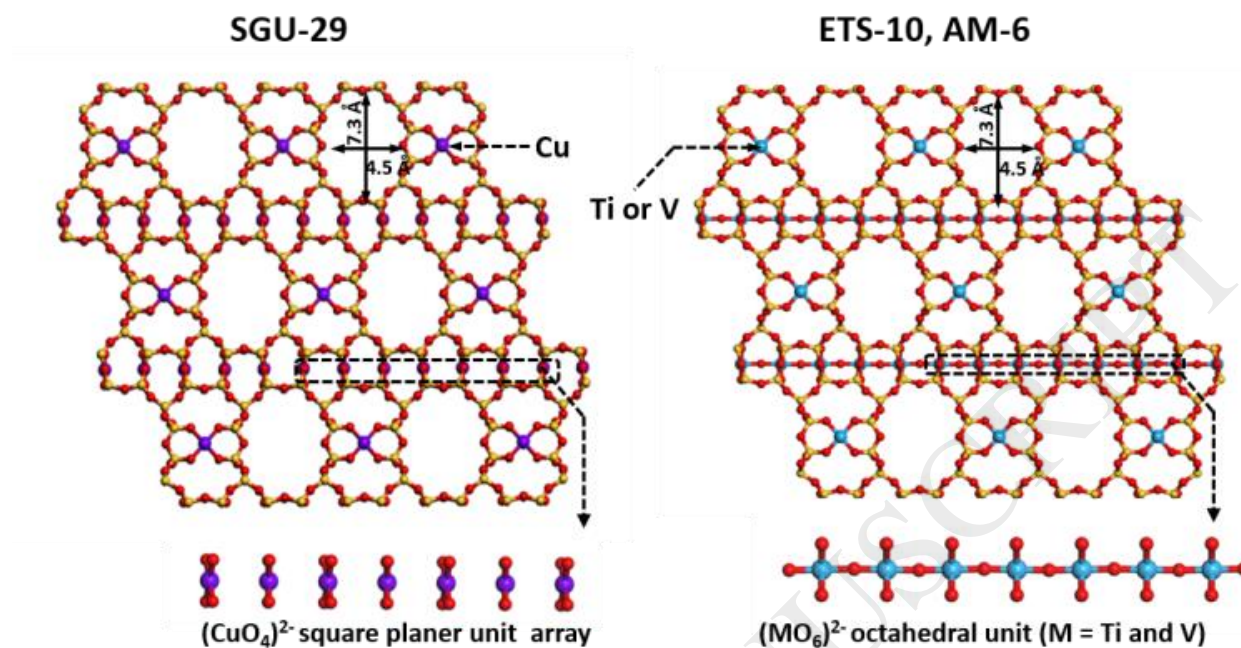**Figure 1**. Schematic structural illustration of (left side) SGU−29 with [CuO$_4$] square planar units and (right side) ETS−10 (M=Ti) and AM−6 (M=V) with MO$_6$ octahedral unit
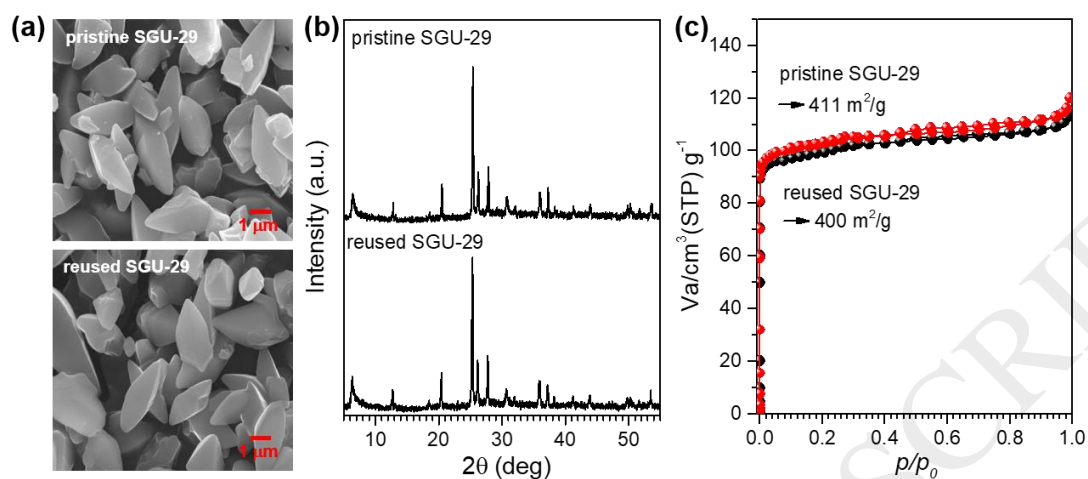
Figure 2. (a) SEM images (b) XRD patterns and (c) surface area from BET analysis of pristine SGU-29 (top) and reused SGU-29 (bottom) after catalytic reaction as indicated.
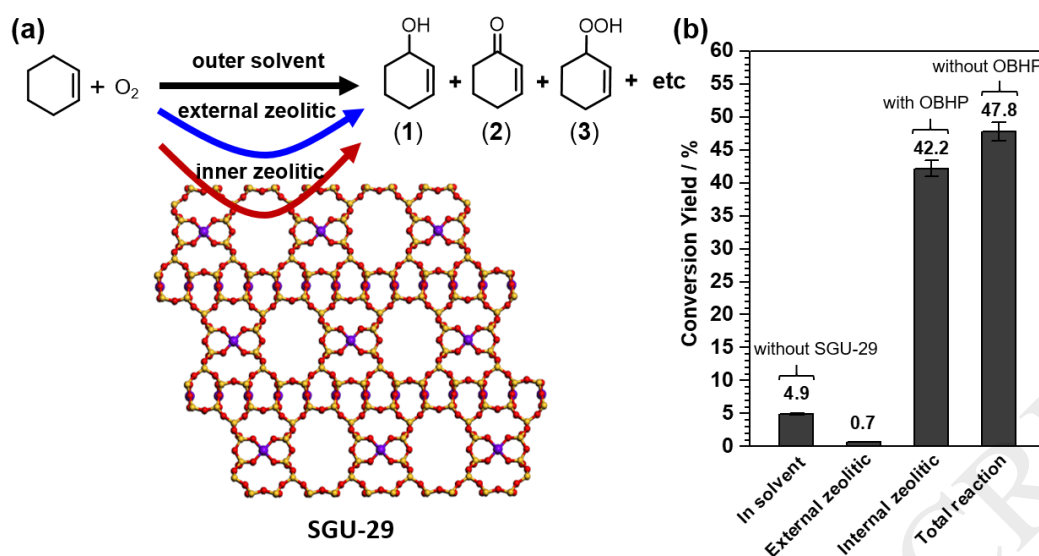
Figure 3. (a) Schematic illustration of possible three places (in solvent, external and inner SGU-29) for cyclohexene aerobic oxidation catalyzed by SGU29 and (b) each conversion yield of indicated three places and total conversion yield. Reaction condition: 4.0g cyclohexene, 4.8g acetonitrile, 1.0g toluene (internal standard), 0.1g octadecyl–3–(3,5–di–tertbutyl–4–hydroxyphenyl)–propionate (OBHP, bulky scavanger) and 10mg catalyst. Conversion yield = (amount of initial cyclohexene – amount of cyclohexene after reaction)/amount of initial cyclohexene.
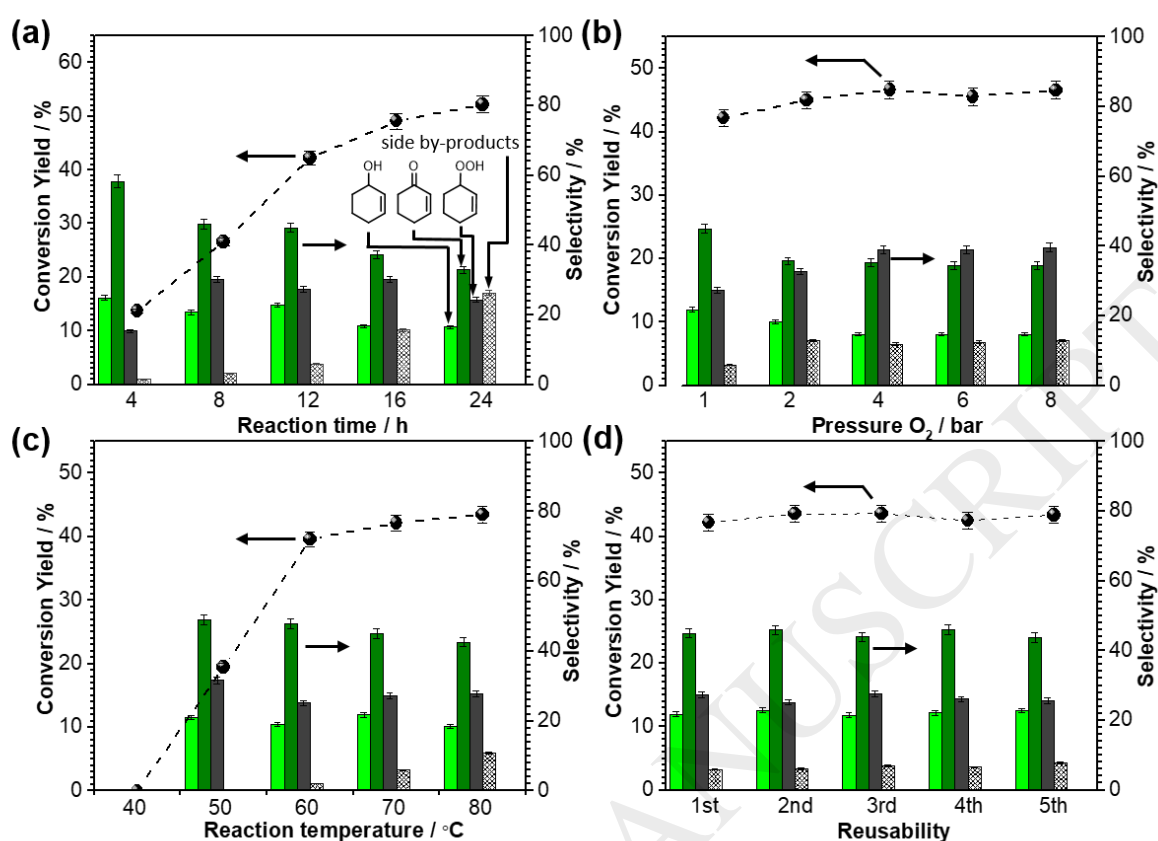
Figure 4. Conversion yield and product selectivity for aerobic oxidation of cyclohexene-catalyzed SGU–29 dependences on (a) reaction time (b) O2 pressure (c) reaction temperature, and (d) reusability of the SGU–29. Reaction condition: 4.0g cyclohexene, 4.8g acetonitrile, 1.0g toluene (internal standard), 0.1g octadecyl–3–(3,5–di–tertbutyl–4–hydroxyphenyl)–propionate (OBHP, bulky scavanger) and 10mg catalyst. Conversion yield = (amount of initial cyclohexene – amount of cyclohexene after reaction)/amount of initial cyclohexene.
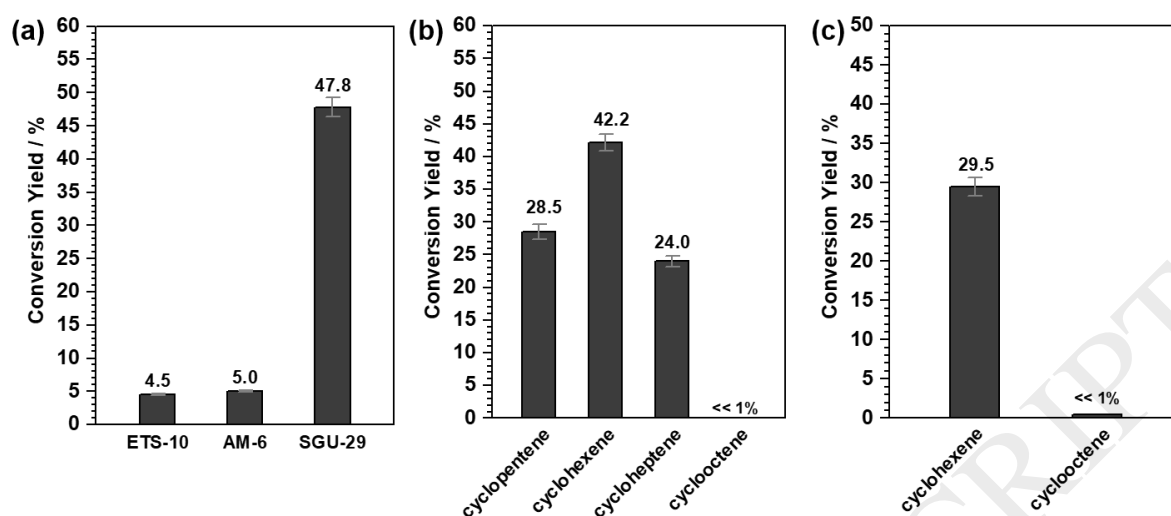
Figure 5. (a) Comparison of conversion yields of ETS-10, AM-6 and SGU-29 for aerobic oxidation without OBHP, (b) various cycloalkane and (c) reactant mixture of 1:1 cyclohexene and cis-cyclooctene as indicated. Reaction condition: 4.0g cyclohexene, 4.8g acetonitrile, 1.0g toluene (internal standard), 0.1g octadecyl–3–(3,5–di–tertbutyl–4–hydroxyphenyl)–propionate (OBHP, bulky scavanger) and 10mg catalyst. Conversion yield = (amount of initial cyclohexene – amount of cyclohexene after reaction)/amount of initial cyclohexene.
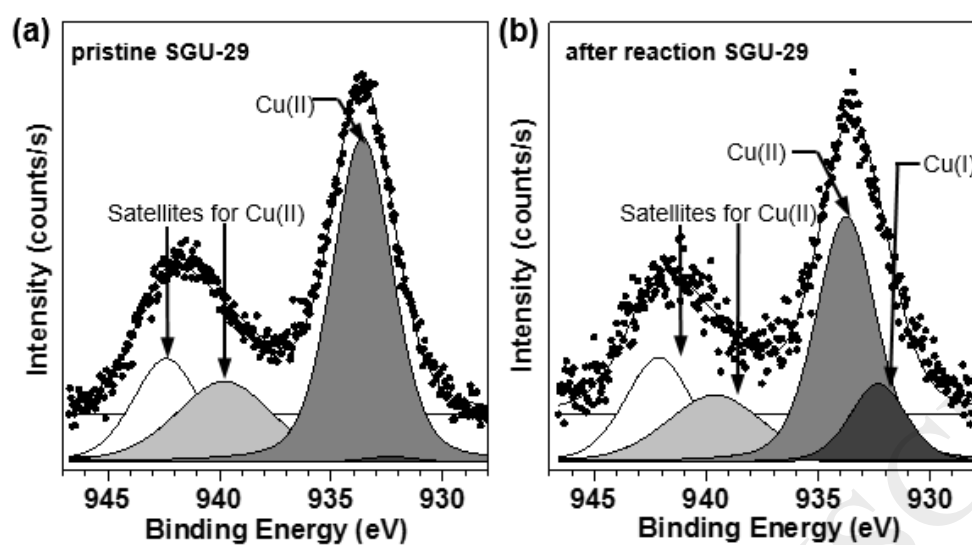
Figure 6. XPS Cu 2p$_{3/2}$ spectra of CuO$_4^{2-}$ in SGU–29 (a) as prepared and (b) after five catalytic cycles (reaction conditions: 1 bar of O^2 at 70°C for 12 h)
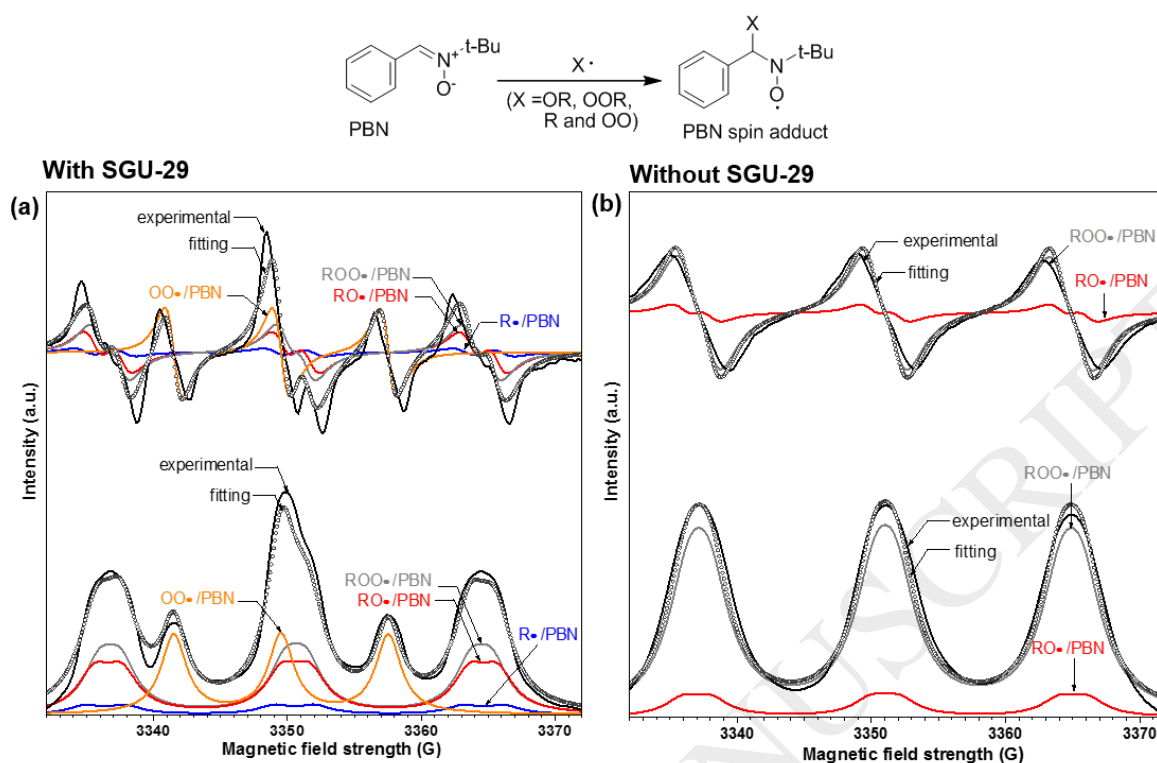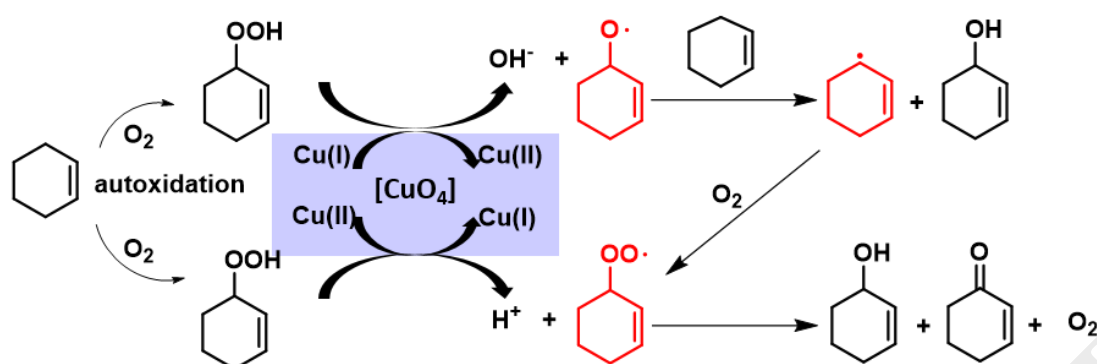
Figure 7. ESR absorption spectra (upper) and the collected first derivative spectra (lower) of the observed PBN spin adducts in catalytic reaction with (a) and without (b) SGU–29, as indicated

Scheme 1. Proposed pathway for the aerobic oxidation of cyclohexene by SGU–29 and radical species (red) generated during oxidation.
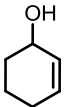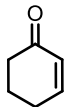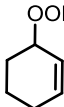
Entry	Catalyst	Time/h	O_2 /bar	Temperature /°C	Conversion[b]/%	Selectivity[c]/%			
						OH	O	OOH	side-by-products[d]
1	SGU-29	4	1	70	13.7	25.8	58.3	15.4	1.5
2	SGU-29	8	1	70	26.6	24.6	49.2	23.1	3.1
3	SGU-29	12	1	70	42.2	23.3	47.7	29.0	5.9
4	SGU-29	16	1	70	49.1	16.7	37.4	30.2	15.7
5	SGU-29	24	1	70	52.2	16.5	32.9	24.3	26.3
6	SGU-29	12	2	70	45.0	18.4	35.8	32.7	12.9
7	SGU-29	12	4	70	46.7	14.7	35.2	39.0	12.0
8	SGU-29	12	6	70	46.5	14.6	34.3	38.9	12.4
9	SGU-29	12	8	70	46.6	14.9	34.4	39.6	12.9
10	SGU-29	12	1	40	~0	-	-	-	-
11	SGU-29	12	1	50	19.5	31.7	48.9	19.0	0.4
12	SGU-29	12	1	60	39.6	24.0	47.8	24.1	2.1
13	SGU-29	2	1	80	43.5	19.1	42.5	27.7	10.7
14	SGU-29[e]	12	1	70	47.8	20.1	46.4	27.5	6.0
15	ETS-10[e]	12	1	70	4.5	5.9	14.8	79.3	-
16	AM-6[e]	12	1	70	5.0	6.4	13.5	80.1	-
17	Blank[e]	12	1	70	4.9	6.2	12.4	81.5	-

Table 1. Conversion yields and products selectivity for aerobic oxidation of cylclohexene in this work[a].
[a] reaction condition: 4.0g cyclohexene, 4.8g acetonitrile, 1.0g toluene (internal standard), 0.1g octadecyl–3–(3,5–di–tertbutyl–4–hydroxyphenyl)–propionate (OBHP, bulky scavanger) and 10mg catalyst.
[b] conversion yield:(amount of initial cyclohexene − amount of cyclohexene after reaction)/amount of initial cyclohexene.
[c] selectivity: amount of individual product/ amount of consumed cyclohexene
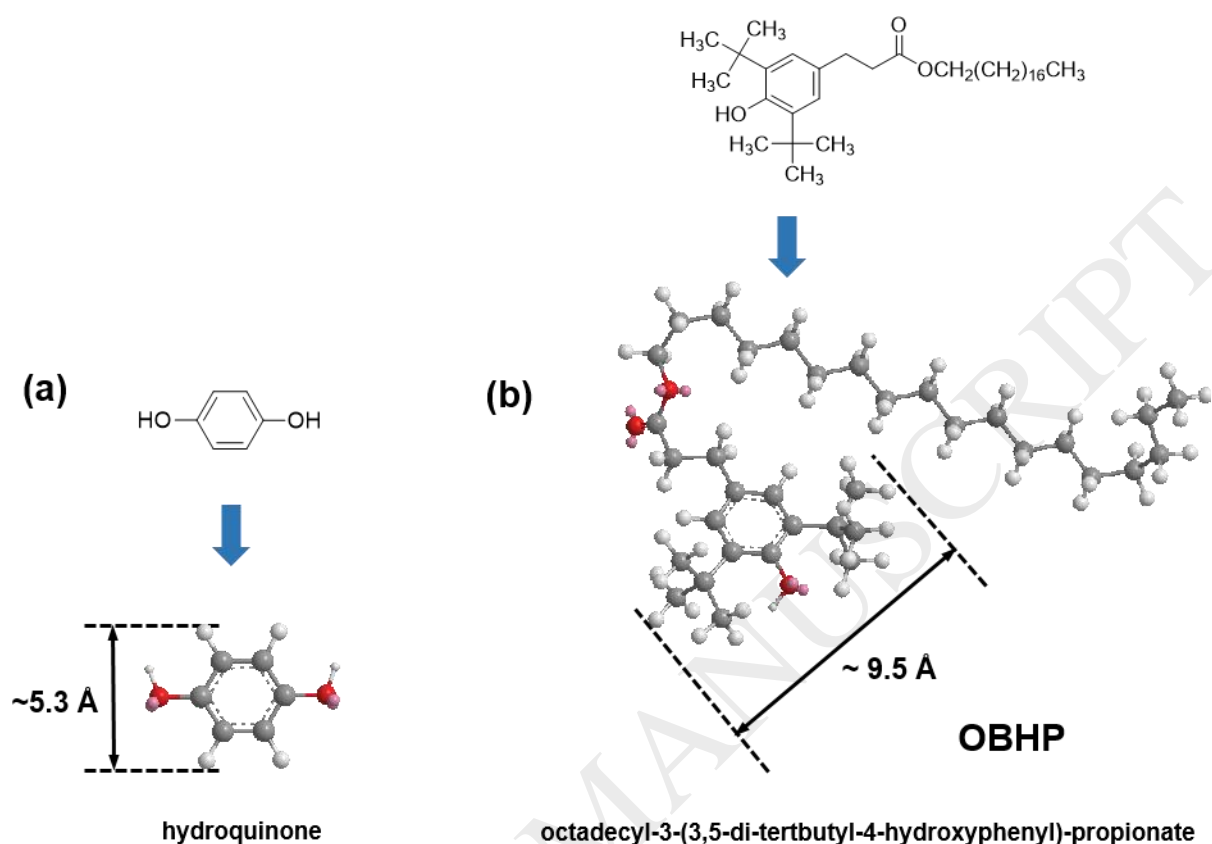[d] (amount of consumed cyclohexene − amount of three main products)/ amount of consumed cyclohexene
[e] catalytic reaction without OBHP

Supplementary material

Contents
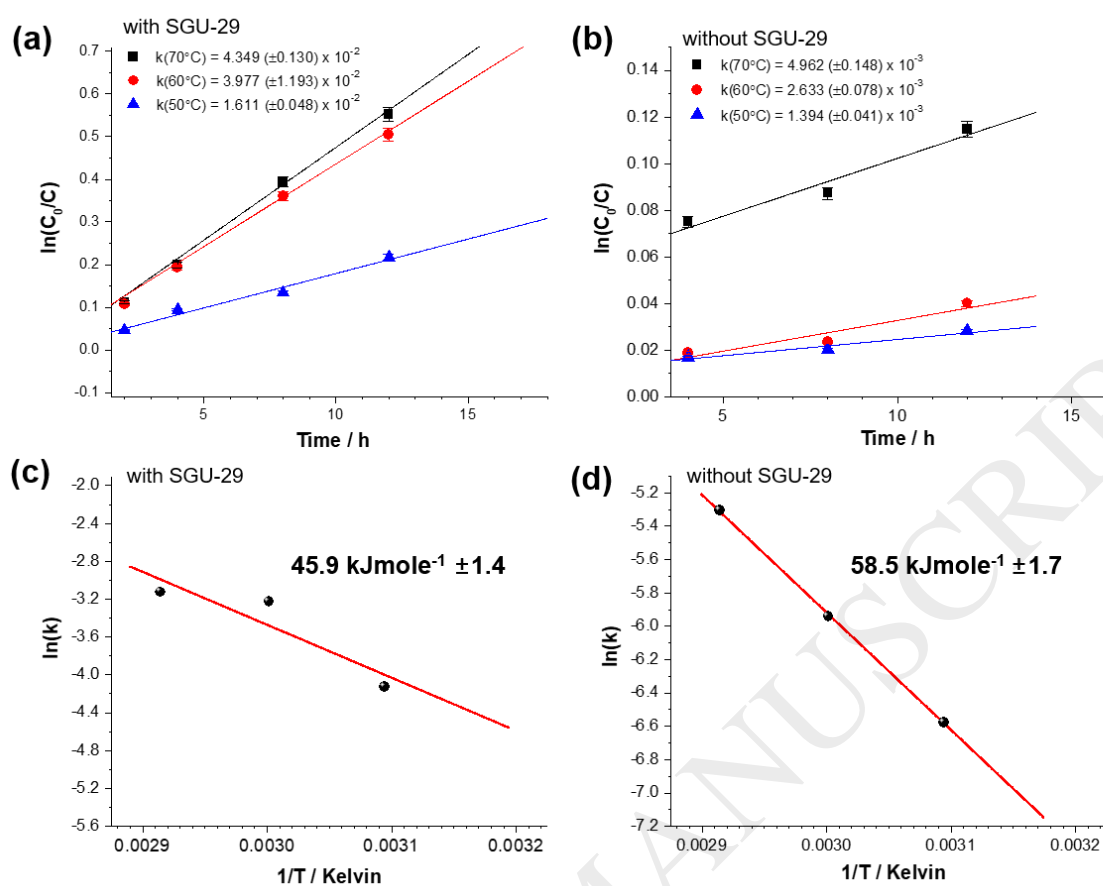
S1. Estimated size of (a) hydroquinone and (b) OBHP (octadecyl–3–(3,5–di–tertbutyl–4–hydroxyphenyl)–propionate) used as scavengers in this study as indicated: The chemical structures of molecules were first drawn by ChemDraw Ultra 12.0 and then the structure files were imported into Chem3D Ultra 12.0. The chemical structures of scanvangers were optimized by the process Molecular Mechanics 2 (MM2) Minimize Energy. Minimum RMS Gradient was set to 0.01 from ChemDraw3D structures after MM.
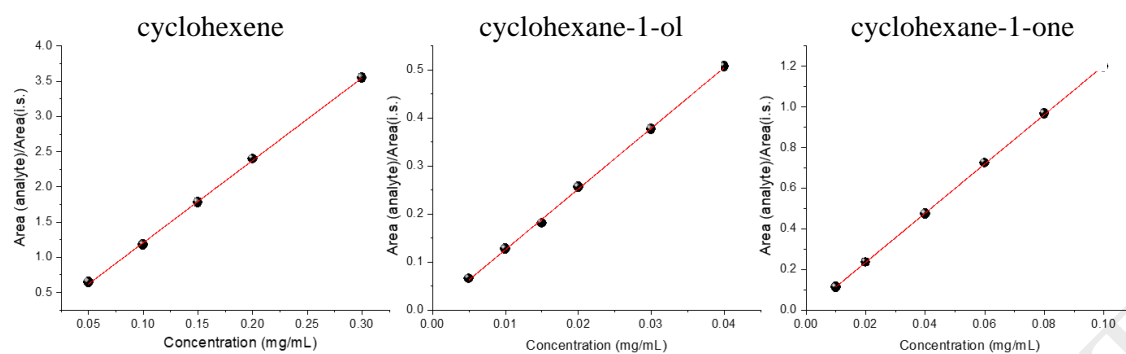
S2. Calibration curve for cyclohexene, cyclohexane-1-ol and cyclohexane-1-one products.

(a) with SGU-29

- $k(70°C) = 4.349 \ (\pm0.130) \times 10^{-2}$
- $k(60°C) = 3.977 \ (\pm1.193) \times 10^{-2}$
- $k(50°C) = 1.611 \ (\pm0.048) \times 10^{-2}$

(b) without SGU-29

- $k(70°C) = 4.962 \ (\pm0.148) \times 10^{-3}$
- $k(60°C) = 2.633 \ (\pm0.078) \times 10^{-3}$
- $k(50°C) = 1.394 \ (\pm0.041) \times 10^{-3}$

(c) with SGU-29

$45.9 \ \text{kJmole}^{-1} \ \pm1.4$

(d) without SGU-29

$58.5 \ \text{kJmole}^{-1} \ \pm1.7$

S3. Plots between $\ln(C/C_0)$ *vs.* time (a) with and (b) without SGU-29, and Arrhenius plots for aerobic oxidation (c) with and (d) without SGU-29

S4. Calculation TON and TOF

(1) The unit cell composition of pristine SGU-29 is $Na_{1.15}K_{0.84}CuSi_5O_{12}$

(2) The number of water molecules contained in SGU-29 was obtained from TGA analysis. The portion (weight loss % is 5.5% as indicated), between 50 °C and 300 °C represents desorption of loosely bound SGU-29 water. So the actual weight could be calculated to be 9.45mg by subtracting from10mg of SGU-29 to the amount of water, 0.55mg.
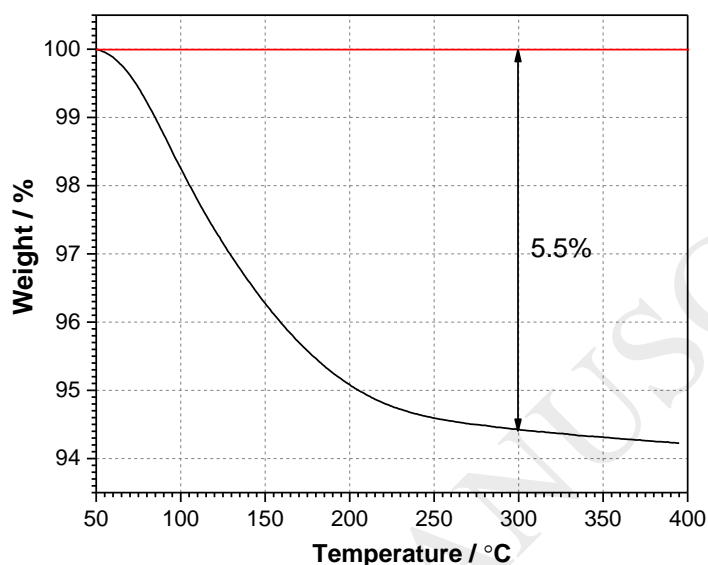
(3) Molecular weight of SGU-29's unit cell

→ 455.25g·mol^{-1}

(4) The number of square unit, [CuO$_4$] in 9.45mg of SGU-29

$$\rightarrow \frac{9.45\ mg}{455.25g \cdot mole^{-1}} = 2.08 \times 10^{-5}\ mole$$

(5) The number of consumed cyclohexene

→ conversion yield (42.2 %) × initial mole of cyclohexene (4.00g, MW: 82.14g·mol^{-1})

= 2.05 × 10^{-2} mole

(6) Turnover Number (TON) using 9.45mg of SGU-29 (under1 bar of O$_2$ at 343 K for 12 h)

$$\rightarrow \frac{The\ number\ of\ consumed\ cyclohexene}{number\ of\ CuO4^{2-}\ in\ 10mg\ of\ SGU-29} = \frac{2.05 \times 10^{-2}\ mole\ from\ (5)}{2.08 \times 10^{-5}\ mole\ from\ (4)} = 985.6$$

(7) Turnover Number (TON) using 9.45mg of SGU-29 (1 bar of O$_2$ at 343 K for 12 h)

→ Turnover Number (TON)/ reaction time (h) = 985.6/12h = 82.1h^{-1}
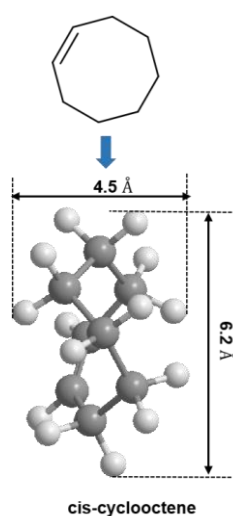
cis-cyclooctene

S5. Estimated size of cis-cyclooctene: The chemical structures of molecules were first drawn by ChemDraw Ultra 12.0 and then the structure files were imported into Chem3D Ultra 12.0. The chemical structures of scanvangers were optimized by the process Molecular Mechanics 2 (MM2) Minimize Energy. Minimum RMS Gradient was set to 0.01 from ChemDraw3D structures after MM.

Table S1. The Performance of cyclohexene aerobic oxidation using various catalyst based on the porous materials

Catalyst	Time /h	O_2 /bar	Temperature /℃	Conversion/ %	TON[a]	Ref
SGU-29	12	1	70	42.2	**986**	This work
$[Fe(bpy)_3]^{2+}$@Zeolite Y	24	O_2 atmosphere	50	-	**46**	23
Ni-MOF $[Ni_2(DOBDC)(H_2O)_2]\cdot 8H_2O$	20	O_2 balloon	80	13.2	**65[b]**	28
Co-MOF $[Co_2(DOBDC)(H_2O)_2]\cdot 8H_2O$	10	O_2 balloon	80	8.1	**39[b]**	28
Cu-MOF $[Cu_2(OH)(BTC)(H_2O)]_n\cdot 2nH_2O$	10	O_2 balloon	80	11.7	**57[b]**	28
Cu-MOF $Cu(bpy)(H_2O)_2(BF_4)_2(bpy)$	15	O_2 balloon	45	-	**37**	S1
Cu^{2+}@COMOC- 4	7	O_2 flow	40	49.0	**150[b]**	S2
$[Co^{II}Co_2^{III}(\mu_3\text{-}O)\text{-}bdc)_3(tpt)]\cdot 4DMF\cdot 3H_2O$	24	1	70	37.9	**137**	13
CU-MOF $[Cu_2(bipy)_2(btec)]$	6	O_2 atmosphere	75	15	**36[b]**	15
SiO_2/Al_2O_3-APTMS-BPK-Mn(III).	24	O_2 balloon	120	97[c]	**55.42**	S3

[a] The number of converted cyclohexene / number of catalytic site

[b] calculated based on conversion and moles of catalyst

[c] N-hydroxyphthalimide (NHPI) additive contained condition

S1. D. Jiang, T. Mallat, D.M. Meier, A. Urakawa, A. Baiker, J. Catal. 270 (2010) 26–33

S2 Y.-Y. Liu, K. Leus, T. Bogaerts, K. Hemelsoet, E. Bruneel, V. Van Speybroeck, P. Van Der Voort, ChemCatChem 5 (2013) 3657–3664.

S3 D. Habibi, A. Faraji, M. Arshadi, H. Veisi, A. Gil, J. Mol. Catal. A: Chem. 382 (2014) 41–54.

Table S2. ESR hyperfine constants of formed PBN adducts.

Radical Adduct	Hyperfine coupling constants/G	
	A_N	A_H
ROO•/PBN	13.88	1.58
RO•/PBN	14.03	2.06
R•/PBN	14.14	3.00
O•/PBN	8.02	-